Nanobiotechnol (2007) 3:46–54
DOI 10.1007/s12030-007-0006-2

Quantitative Detection of Engineered Nanoparticles in Tissues and Organs: An Investigation of Efficacy and Linear Dynamic Ranges Using ICP-AES

Hans C. Fischer · Sébastien Fournier-Bidoz · K. Sandy Pang · Warren C. W. Chan

Published online: 30 June 2007

Abstract The absence of effective non-isotopic quantification methods to determine *in vivo* nanoparticle kinetics and distribution is a key obstacle to the development of various biomedical nanotechnologies. This paper presents a novel adaptation of the established technology of Inductively Coupled Plasma-Atomic Emission Spectroscopy (ICP-AES) to a simple technique intended to address this obstacle. Applicability to three varieties of nanoparticles, (CdSe/ZnS quantum dots (QD), gold nanoparticles, and Fe_3O_4 nanoparticles) was investigated, and particle detection sensitivity was shown in moles of particles per gram of tissue. Using gold nanoparticles, increased particle size corresponded with lower molar detection thresholds. Minimum linear detection ranges of 2.5 orders of magnitude for QDs and 1.5 orders of magnitude for all three sizes of gold were demonstrated. The detection of the Fe_3O_4 particles was hampered by the natural presence of Fe^{2+} in tissues, showing that the technique is not suitable for measuring nanoparticles composed of endogenous elements. These detection levels and ranges demonstrate that this technique is useful for quantifying nanoparticles in excised organs, after *in vivo* dosing.

Keywords nanoparticle · *in vivo* quantitation · quantum dot · ICP-AES · non-isotopic detection

H. C. Fischer · S. Fournier-Bidoz · W. C. W. Chan (✉)
Department of Materials Science and Engineering,
Institute of Biomaterials and Biomedical Engineering,
Terrence Donnelly Center for Cellular and Biomolecular Research,
University of Toronto, Toronto, Ontario M5S 3G9, Canada
e-mail: warren.chan@utoronto.ca

K. S. Pang
Leslie Dan Faculty of Pharmacy, University of Toronto,
Toronto, Ontario M5S 3M2, Canada

Introduction

Many promising biomedical applications using nanoparticles have been conceptualized in the last decade. These are exemplified by the use of semiconductor and metallic nanoparticles in cancer detection and treatment [1–3], which inherently requires intravenous exposure to nanoparticles. A dependable quantification method is vital to refining, tailoring, and developing these technologies to advance them toward clinical uses [4]. A suitable method must be capable, by quantifying nanoparticles in tissues and organs, of characterizing the distribution, pharmacokinetics, clearance, metabolism, and response of the body to various nanoparticles. The traditional method of radiolabeling may be used for nanoparticles such as carbon nanotubes [5] and polymer nanoparticles [6], but may be inappropriate for many other engineered nanoparticles such as semiconductor quantum dots (e.g., CdSe, HgS, PbSe) and metallic nanoparticles (e.g., Ag, Ni, Co). It would be very difficult to radiolabel some of these nanoparticles because of the high molecular weight synthetic precursors and the potential hazards of the synthetic conditions, which use pyrophoric precursors at >300 °C [7].

Although there exists a significant body of literature describing the *in vivo* distribution of readily quantifiable radio-colloids, the results may not fully describe the pharmacokinetic properties of engineered nanoparticles. Modern colloids are smaller and designed with three major components: 1) core nanoparticles, 2) coated with stabilizing molecules, and/or 3) coated with biological molecules. Radiolabeling of the surface molecule coating on the core nanoparticle is easily achieved, but the pharmacokinetic data using this labeling scheme can be misleading because of the *in vivo* metabolic trajectory of the labeled compound (which may differ from the core nanoparticle). A recent

example of this is data pertaining to the excretion of carbon nanotubes in urine [5]. TEM micrographs showed urinary excretion of the carbon nanotubes, but corresponding scintillation values were conspicuously absent, suggesting that the ^{111}In label may or may not be excreted in conjunction with the nanotubes. Quantification of the ligands on surface radiolabeled nanostructures is not a reliable strategy to quantitatively deduce their fate, as ultimately it is the core, or body, of the nanoparticle, which is of most investigative interest. A surface tag would provide information pertaining to the location of desorbed ligands and their metabolites, not the core. Despite the important role that the surface coating plays in influencing the *in vivo* disposition [8–10], the overall residence time and fate of the nanoparticle core are of principle interest.

A study on whole body distribution of one type of nanoparticles—ZnS-capped CdSe semiconductor quantum dots—has been described qualitatively in mice [11], and the authors based their conclusions on the observation of photoluminescence, which is known to vary according to the type and status of adsorbed molecules on the surface [10]. Use of inappropriate quantitation methods such as this can drastically over- or under-represent the actual quantum dot quantity present. These factors illustrate why many engineered nanoparticles lack a reasonable method for *in vivo* quantification. There is a corresponding scarcity of nanoparticle distribution and pharmacokinetic studies in animals.

Studies that describe the pharmacokinetics and whole body distribution of administered nanoparticle technologies *in vivo* have been successfully completed, the observations of which clearly show the influence of chemical design of the nanoparticles on their *in vivo* activities [8]. Therefore, it is of pivotal importance to develop a tool that can thoroughly quantify the activities of engineered nanoparticles for assessment of the impact of chemical alterations on biological function, and determine the extent of any deleterious effects for the advancement of nanotechnology.

We present an accessible adaptation of established techniques of Inductively Coupled Plasma-Atomic Emission Spectroscopy (ICP-AES) as a method suitable for the quantification of nanoparticles in organ matrices pertinent to *in vivo* distribution research. The method presented must also accommodate the large number of samples involved in analyzing organ samples for the determination of pharmacokinetic parameters at subnanomole quantities of nanoparticles. We investigated the applicability of the technique to a variety of nanoparticle types and sizes and how effective the method is in dealing with elemental background levels. To achieve this, semiconductor quantum dots (ZnS capped CdSe), which are useful as contrast agents for optical *in vivo* imaging [1, 12], were used. Gold nanoparticles were chosen for this study because of their demonstrated usefulness for drug delivery and targeted hyperthermia [2]. Magnetite nanoparticles (Fe_3O_4), which are commonly used as MRI contrast agents or hyperthermia agents, were included [13] as an example of a nanoparticle composed of a quantifiable element metric, which has substantial endogenous levels in tissue. To provide an outline of a successful analytical technique useful for quantifying *in vivo* nanoparticle kinetics, we present data detailing the limits of detection, the linear range, and tissue sample volumes at which matrix interference becomes a significant factor.

Results and Discussion

Nanoparticles Used

Nanoparticles were synthesized and purified according to the protocols referenced above, and the surface coating

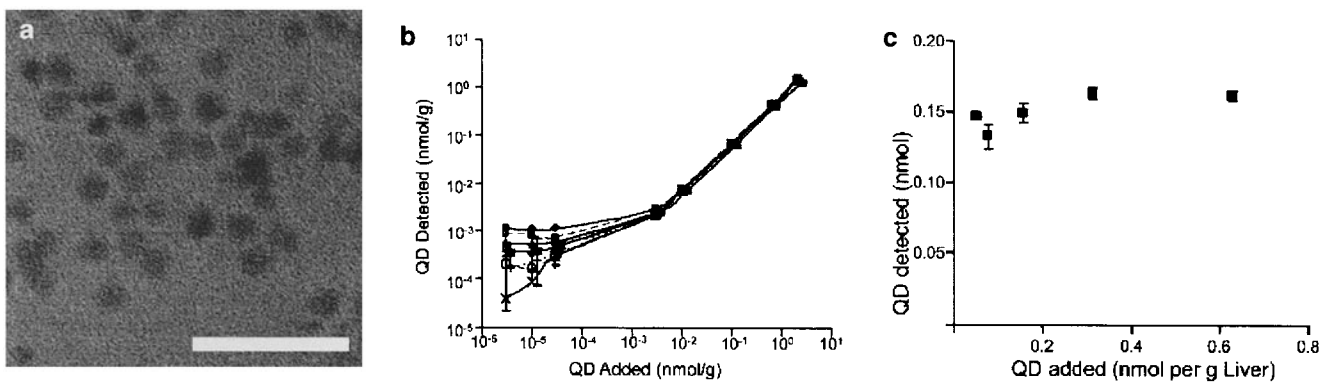

Fig. 1 Measurements of semiconductor nanocrystal QDs in tissues using ICP-AES. The TEM image (**a**) shows a monodisperse sample (scale bar=30 nm). (**b**) Linear dynamic range plot showing the limit of QD detection in various tissues (nmol g^{-1} tissue). The upper detection saturation limit has not been reached. A detection threshold of 10^{-2} nmol g^{-1}, and minimum linear range of 2.5 orders of magnitude are shown (▲ liver; □ lung; ♦ brain; ■ spleen; ◇ kidney; + heart; × muscle; ○ skin). (**c**) The interference effect of tissue quantity on detection efficiency is shown by the deviation of the data points from a horizontal trend, which indicates the quantity of QD added

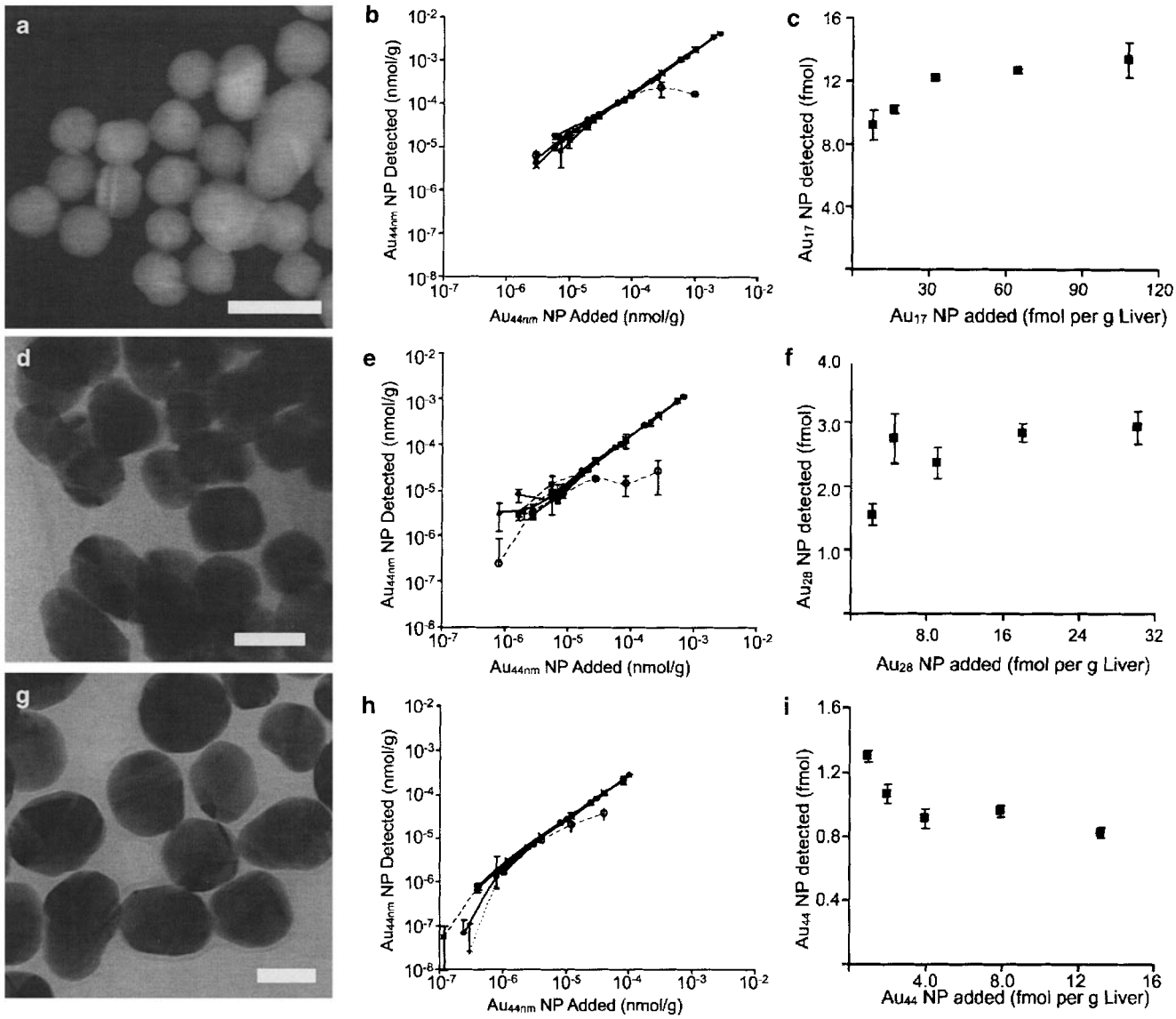

Fig. 2 Measurements of three different sized gold nanoparticles in tissues using ICP-AES. The TEM images (**a**, **d**, and **g**) show monodisperse nanoparticles (scale bars=30 nm). Linear range plots (**b**, **e**, and **h**) showing the limit of gold nanoparticle detection in various tissues (nmol g^{-1} tissue). The upper detection saturation limit has not been reached. A detection threshold of $10^{-4.0}$, $10^{-4.5}$, and $10^{-5.0}$ nmol g^{-1}, and minimum linear range of 2.5 orders of magnitude are shown for 17, 28, and 44-nm-diameter gold nanoparticles, respectively (▲ liver; □ lung; ♦ brain; ■ spleen; ◇ kidney; + heart; × muscle; ○ skin). The interference effect of tissue quantity on detection efficiency (**c**) is shown by the deviation of the data points from a horizontal trend, which indicates the quantity of gold nanoparticles added

properties have been described [14–17]. The diameter and monodispersity of the nanoparticle samples were confirmed by optical absorbance and by transmission and Z-contrast electron microscopy (TEM). See Figs. 1a; 2a,d, and g; 3a. Images were taken using a Hitachi HD2000 STEM. Mean particle diameter and standard deviation were calculated from measurements taken from the images using Imagepro software (MediaCybernetics). The QDs used were measured to be 5.01±0.61 nm; the three sizes of gold nanoparticles used were 17.3±2.0 nm, 27.7±4.2 nm, and 43.8±7.1 nm; the Fe_3O_4 particles were 6.1±1.4 nm. Based on the TEM images, the nanoparticles in each sample were essentially spherical. The difference in electron density between the QDs and the gold nanoparticles is evident by the high contrast achievable in the gold images. The apparent aggregation observed in Fig. 3a is likely caused by the magnetic interaction between the particles during sample drying.

Digestion of Nanoparticles

The procedure used in this work for wet mineralization of the samples was adapted from existing techniques, but

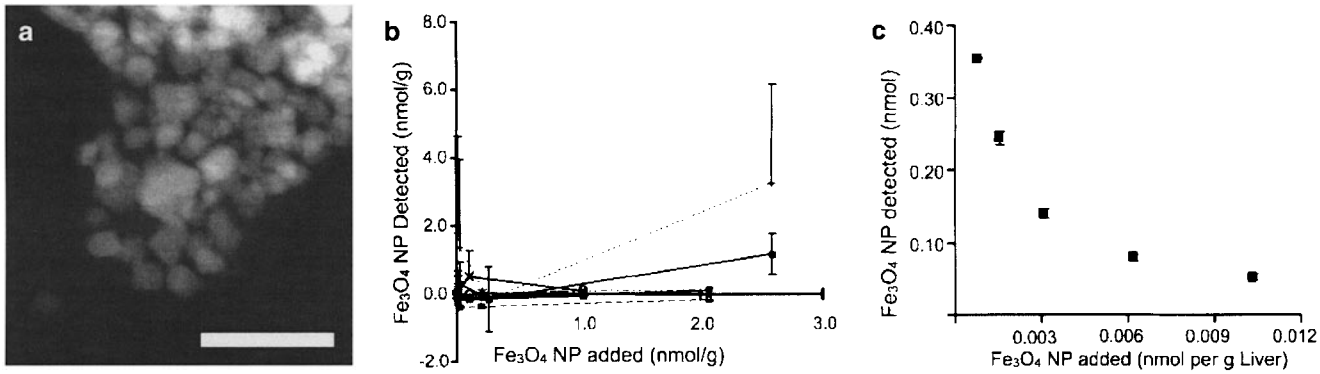

Fig. 3 Measurements of Fe3O4 nanoparticles in tissues using ICP-AES. (**a**) TEM image shows a single nanoparticle with some clustering (scale bar=30 nm). (**b**) Graph shows that the variability of Fe in the tissues obstructs the detection of nanoparticles present (▲ liver; □ lung; ♦ brain; ■ spleen; ◇ kidney; + heart; × muscle; ○ skin). Additionally, the interference effect of tissue quantity added is clear (**c**), shown by the incremental increase of Fe present in the samples as more liver tissue was added. Nanomolar values expressed are calculated from the amount of Fe per nanomole of nanoparticles, and do not indicate that particles are being generated in the prepared sample

modified to accommodate large sets of samples. For analyzing nanoparticles in tissues, we found that the simple use of concentrated nitric acid (HNO_3) is enough to digest the tissues for ICP-AES analysis. Confirmation of the efficacy of the digestion technique described was shown by the detection of a known quantity of each element to be investigated, after digestion in combination with liver tissue homogenate. The cadmium, gold, and iron were added in the form of aqueous standards with certified concentrations. The percent of each element, determined by ICP-AES measurements, remaining in the sample after digestion was 87.0±11.4% for Cd, 85.1±12.6% for Au, and 170.0± 11.7% for Fe. Except for Fe_3O_4, which expectedly has greater than 100% because of the Fe content of liver tissue. The fraction not recovered likely nonspecifically adhered to container walls during sample processing, or evaporated as a result of high vapor pressure in the case of Cd. The variability associated with the recovery values is not high enough to interfere with the intended application, in which the relative quantity measured describes the pharmacokinetic parameters rather than the absolute initial content.

Experiments on the nanoparticles alone were performed to correlate elemental content to particle number. Complete digestion of the nanoparticles was achieved. This was evidenced by the fact that both QDs and gold nanoparticles have optical properties (photoluminescence, and solution coloration caused by absorption, respectively) which were not observed after digestion, indicating that nanoparticles were no longer present.

Typically, for most digestion experiments involving tissues for ICP-AES analysis, HNO_3 digestion of tissue samples is combined with elevated pressure or microwave digestion techniques to achieve higher temperatures for maximal digestion. However, this technique utilizes specialized equipment and is time consuming and therefore, will be difficult for pharmacokinetic analysis (where hundreds to thousands of samples per study are required for digestion).

Determining Sensitivity and Linear Dynamic Range of Nanoparticles in Tissues

The ICP-AES measurements were correlated to nanoparticle concentration by two methods. Intact QD and gold nanoparticles have molar extinction coefficients and therefore, we express our data in nanomole of nanoparticles per gram of tissue. QD concentration was determined by initially obtaining a UV–vis absorption spectrum, followed by calculation using Beer's law based on the extinction coefficient derived from Yu et al. [18]. For the gold nanoparticles, the extinction coefficients were determined experimentally based on atomic lattice packing, as described by Chithrani et al. [19]. The magnetite nanoparticles had no discernable UV–vis absorption feature that could be satisfactorily applied to the quantification of the nanoparticles. The relationship between nanoparticle concentration and Fe content was calculated from the ICP-AES data using literature values for Fe_3O_4 crystal structure and density [20].

Among all the investigated nanoparticle types, the type of tissue into which nanoparticles distribute does not affect the detectability. This is shown, within the linear region in each of Fig. 1b, Fig. 2b,e, and h, by the fact that all the data points for a given quantity of NP added are superimposed. This indicates that there is no discrepancy in the effect of different tissues on the efficacy of the sample digestion and preparation process. The apparent density of data points is a reflection of the log/log presentation of results. The slight abscissal offset between the points results from the slight difference in tissue amount added for different organs in accordance with the significant difference in relative organ size in rats. The errors (1 S.D.), although present, are low. The leveling and scatter of data

Table 1 Detection thresholds for various nanoparticles, and demonstrated minimum linear ranges.

	QD CdSe/ZnS	Au NP 17 nm	Au NP 28 nm	Au NP 44 nm	Fe_3O_4 NP
Detection threshold (nmol g^{-1})	$10^{-2.0}$	$10^{-4.0}$	$10^{-4.5}$	$10^{-5.0}$	>2
Demonstrated range (orders of magnitude)	2.5	1.5	1.5	1.5	N/A

points observed at the left of Fig. 1b and Fig. 2b,e, and h are the result of instrument noise at the low end of its detection range. The observed linear ranges in Figs. 1 and 2, (the minimum ranges are tabulated in Table 1) are expected to continue to the saturation limit of the instrument. The thresholds and ranges in Table 1 are, except for tests using gold nanoparticles in skin, broadly representative of detection in any of the tissues used. The minimal difference between tissue data sets makes this possible. Important to note is that because of the variability of nanoparticle batches, positive controls and batch-specific calibration curves are necessary in any application of this assay.

ICP-AES data is typically presented in μg/L, or parts per billion (ppb) units. Data from our work have been presented in units of nanomole per gram of tissue, as this unit is more useful for the task of accounting for intact nanoparticles in biological samples such as excised tissues. As an example of the relationship between measured ppb values and the nanomole per gram (nmol/g) data presented, in the case of QDs Cd detected at 5 ppb corresponds to 0.003 nmol QDs per gram of tissue.

Quantum Dots

Different elements are associated with different ICP-AES detection thresholds, and exhibit differing susceptibilities to error. For example, cadmium and many other metals may be easily measured by ICP-AES because these are present in very low quantities in biological tissues and organs, thus yielding very low background signals. Also, the documented high sensitivity and minimal spectral interference between Cd and tissue allows for the detection of low levels of metallic ions. Our results therefore, shown in Fig. 1, demonstrate that it is possible to detect QDs in tissue in the order of 10^{-2} nmol g^{-1} of tissue, and for at least 2.5 orders of magnitude.

Gold

Although gold nanoparticles may be successfully quantified with radiolabeling [21, 22], we found that ICP-AES was also effective for measuring gold nanoparticles contained in tissue, with good sensitivity. This is valuable in that the same technique can be applied to different types of nanoparticles, including varieties that do not lend themselves to radiolabeling, as mentioned above. Each of the three sizes of gold nanoparticles used was comparable in terms of shape and morphology (Fig. 2a,d,g). The observed shift in detection range between Fig. 2b,e, and h represents an expected manifestation of the different quantities of gold atoms contained within nanoparticles of different sizes. The detection range cited is the same (a minimum range of 1.5 orders of magnitude) for all sizes because of experimental design and availability of nanoparticle sample.

A key to analyzing gold nanoparticles in tissues is that, once digested with HNO_3, samples need to be analyzed soon after digestion (within the same day) to avoid adsorption of aqueous gold to polymer containers, and losses, which result in variably diminished detection levels [23, 24]. The 44-nm-diameter gold nanoparticles exhibited the lowest detection threshold, at $10^{-5.0}$ nmol g^{-1} compared to 28-nm-diameter gold nanoparticles with a detection threshold of $10^{-4.5}$ nmol g^{-1}, and 17-nm-diameter gold nanoparticles, with a detection threshold of $10^{-4.0}$ nmol g^{-1}. These observations clearly demonstrate utility of this technique in successfully quantifying different sizes of nanoparticles of similar composition in tissues.

Of concern, however, is the observed deviation from linearity in the detection of all three gold nanoparticle sizes in skin tissue. The observed decrease relative to the other tissues is likely caused by the higher fraction of lipids and solids relative to other tissues. Because all tissues were measured according to mass, those with higher moisture content will digest more readily relative to those with lower water content. It was also observed that samples of tissues with high lipid content, principally the skin, contained some amount of white particulate matter at room temperature, after sample digestion. According to literature, this is not unexpected, even with the use of more highly oxidative environments containing H_2O_2, and commercial open-vessel-focused microwave systems, which give acceptable results as determined by certified reference materials [25].

Fe_3O_4

The detection of magnetite nanoparticles in all tissues was poor. See Fig. 3b. Because of negative values, the data were not presented in log/log format as in Fig. 1b and Fig. 2b.

The negative values were the result of subtraction of the measured Fe content in sample and that of each tissue blank prepared. High variability in measured Fe was observed, shown in Fig. 3b, especially at low particle levels. From these observations, it is readily apparent that the Fe_3O_4 nanoparticles are not ideally suited for this ICP-AES technique because of the high endogenous levels of Fe present in tissues, and the relatively high variability compared to other nanoparticles examined. Endogenous tissue levels of iron vary considerably between tissue types, and also within each tissue. For example, natural iron levels in healthy rats are 24±3.3 μg g^{-1} brain [26], 52.5±2.1 μg g^{-1} heart, 21.2±0.5 μg g^{-1} skeletal muscle [27], 102.4±30 μg g^{-1} liver, 616±258 μg g^{-1} spleen, 95.4±13.8 μg g^{-1} lung, and 77.6±11.4 μg g^{-1} kidney [28]. These variations of iron levels observed in tissues used could be partly caused by differences in the efficacy of exsanguinations as the hemoglobin content (which contains a Fe chelator) in residual blood would also cause variability. It is clear that in the liver and spleen, the organs most important to the sequestration of nanoparticles, the variation of endogenous Fe far exceeds the amount of iron from added nanoparticles. The amounts added were scaled to represent levels equivalent to that of intravenous dosing. This makes it difficult to measure the concentration of magnetite nanoparticles in biological tissues using this technique.

Determining the Effects of Tissue Mass on ICP-AES Measurements

The goal of the second set of experiments was to determine the level at which the ratio of tissue to nanoparticles would cause interference in the measurements. The expected detection values, calculated from added nanoparticle amounts and known element content per nanomole of nanoparticle, are shown in Fig. 1c, and Fig. 2c,f, and i, as solid horizontal lines. With the digestion parameters outlined, observations for the QDs (Fig. 1c) deviated from this line when 1 g liver was added. For gold nanoparticles, the results deviated at 0.25, 0.50, and 0.25 g of liver tissue added for 17, 28, and 44 nm gold nanoparticles, respectively (Fig. 2c,f,i, respectively). For Fe_3O_4 it was not possible to derive any useful information. As expected, the addition of more tissues yielded the detection of more iron.

These results provide a guideline on how much tissue mass should be used for measuring the content of nanoparticles in tissue. This information is important as, in most cases, one would assume that a higher tissue mass should be used to accurately assay for low concentrations of nanoparticles in tissue. But our results suggest that the quantity of tissue mass may interfere with the sensitivity. If, however, better sensitivity is required for small organs such as lymph nodes and bone marrow, techniques such as ICP-MS can provide detection sensitivities two to three orders of magnitude better than ICP-AES.

Conclusions

Ultimately, this work demonstrates that ICP-AES after nitric acid digestion is a viable technique for measuring some engineered nanoparticles in tissue. The useful range for QD detection in tissues presented in this work encompasses the data collected from *in vivo* injections of QD using techniques similar to those presented here. The data ranged from 0.006 nmol QD g^{-1} of heart tissue shortly after injection, to 1.8 nmol QD g^{-1} of spleen tissue after 90 min [8].

It is difficult to correlate our Fe_3O_4 values to those cited in literature, and of questionable use, given the demonstrated unsuitability of our technique to nanoparticles, which contain a biologically prevalent element as the only quantifiable species by ICP-AES.

For QDs and gold nanoparticles, a linear dynamic range was demonstrated, calculated to represent a quantity (moles of nanoparticles per gram of tissue sampled) useful for pharmacokinetic tracking, and direct comparison between various species of nanoparticles. Of note, this technique does not determine whether the nanoparticles are intact or metabolized, but other adjunct analytical techniques may be used in combination with ICP-AES to provide a completely assessed activities of nanoparticles *in vivo*. Our results show that the three varieties of nanoparticles can be detected to a level of 10^{-2} nmol g^{-1} for QDs, 10^{-4} nmol g^{-1} for 17 nm gold NP, $10^{-4.5}$ nmol g^{-1} for 28 nm gold NP, 10^{-5} nmol g^{-1} for 44 nm gold NP, and above at least 2 nmol g^{-1} for Fe_3O_4 magnetic nanoparticles. We also show that different organ tissues caused no significant effect on the level of detection of QDs and gold nanoparticles. It can also be concluded that this technique is not effective for elements, such as Fe, which are naturally present in organ tissues in any significant quantity. Many of the nanoparticles being applied to biomedical applications, however, are composed of elements that do not occur naturally in tissues, making the technique presented here widely applicable.

Experimental Section

Materials

All chemicals were used as purchased without further purification. For the synthesis of quantum dots, dimethyl cadmium was purchased from Strem; trioctylphosphine oxide, trioctylphosphine, bis(trimethyl)siloxythiane, sele-

nium powder, mercaptoundecanoic acid, DL lysine, EDC, DCC, were purchased from Sigma Aldrich. For the synthesis of gold nanoparticles, trisodium citrate, sodium borohydride, and cetyltrimethylammonium bromide (CTAB) were purchased from Fisher Scientific, Canada. Gold tetrachloride ($HAuCl_4 \cdot 3H_2O$) and ascorbic acid were purchased from Sigma Aldrich.

Magnetite particles (Fe_3O_4) were synthesized using ferric triacetylacetonate (Fe(acac)3) and 2-pyrrolidone (Sigma Aldrich). Chloroform, tetrahydrofuran, methanol, acetone, and dimethylsulfoxide were purchased from EMD. Ultrapure water (18 MΩ) from a Millipore system (Marlborough, MA) was used for sample preparation and dilution. Nitric acid 70% (reagent grade) was purchased from Sigma Aldrich.

Rats were obtained from Charles River Laboratories (St Constant, QC). Disposable syringe filters, used for eliminating aggregated nanoparticles from solution, were purchased from Millipore (Bedford, MA). Syringes were obtained from Becton-Dickinson (Franklin Lakes, NJ).

Methods

Quantum dots were synthesized according to established CdSe-ZnS core-shell protocols using organometallic precursors [7]. The post synthesis processing that renders the QDs water soluble was that outlined by Jiang et al. [14]. Orange emitting, (600 nm) 4.25 nm diameter core QD were chosen to render this study comparable to other submitted work [8]. The concentration and extinction coefficient of the final aqueous solution were quantified using UV–Vis optical absorbance, according to Yu et al. [18]. Gold nanoparticles of 17, 28, and 44 nm diameter were synthesized using the citrate reduction method [16, 17]. Chloroauric acid (300 μL of 1%) was added to 30 ml water with varying volumes of 1% citric acid to provide the desired size (600 ml for 14 nm; 240 ml for 43 nm). The solution was stirred while boiling, until the color turned red. STEM imaging (Hitachi HD2000) of the gold nanoparticles on carbon coated copper grids confirmed their sizes. Determination of the extinction coefficient for each size was achieved by measuring the amount of elemental gold in a digested solution of gold nanoparticles. From this value and TEM measurements of the nanoparticle size (assuming them to be spherical), the number of particles responsible for the final [Au] was determined. The calculated extinction coefficients, however, vary relative to literature values [29]. This may be due the assumption, used frequently in such calculations, that all the Au added to the synthesis is present as monodisperse colloidal gold [30]. Careful ICP measurements of a purified solution, which provides an accurate value, have been used in this work.

Fe_3O_4 nanoparticles were synthesized using the procedure developed by Li et al. [15]. A quantitative value of nanoparticle concentration was generated by measuring the amount of iron in a known volume of suspended nanoparticle sample, and comparing it to a calculated value of nanoparticle iron content based on density (5.17 g cm^{-3}). No effective extinction coefficient value could be determined because of the lack of an easily identifiable feature within the UV–vis absorbance curve.

Organ Collection

The organ tissues described in all the experiments were prepared from male Sprague–Dawley rats (425–450 g). The procedures were conducted in accordance with approved protocols of the University of Toronto Animal Care Committee. Ketamine and xylazine were used to induce anesthesia. After cannulation of the right external jugular vein, the abdomen was opened and the vena cava was blocked above the right renal vein. Ice-cold saline was perfused into the body via the jugular vein cannular, exiting the vena cava below the blockage. The quality of the exsanguination was gauged by the residual color in the tissues and in vessels. Additional saline was flushed through until no coloration remained.

The liver, kidneys, spleen, muscle (parts of abdominals), skin with fur, lungs, heart, and the brain were excised. The excised tissues were placed in pre-tared centrifuge vials, weighed, and then kept on ice. Physiological buffer was then added (1:1 *g/v*), and the tissues were homogenized, with the exception of the skin. The tissue samples were stored at −80°C until use.

Table 2 Operating conditions and measurement parameters.

Perkin-Elmer Optima 3000 ICP-AES	
(Cd, Fe, Au determination)	
Sample introduction	
Meinhard nebulizer	
Auxiliary Ar flow (L min^{-1})	0.5
Sample flow (mL min^{-1})	2
Nebulizer gas flow (L min^{-1})	0.8
Plasma	
RF power (W)	1,400
Plasma gas flow (L min^{-1})	15
Measures	
Read delay (s)	15
Integration time (s)	5–10
Replicates	3
Emission lines	
Cd (nm)	228.805
Au (nm)	267.595
Fe (nm)	238.204

Sample Preparation

Two basic experiments were conducted, the first consisting of measuring the linear range and sensitivity threshold for three different types of nanoparticles and the second investigating the interference effect of organ tissue amount on that threshold. All experimental samples, including the control samples of nitric acid alone, nitric acid with blank tissue, nitric acid with the various amounts of nanoparticles without tissue, and nitric acid with elemental standard solution, were prepared in triplicate.

For the linear detection range, differing quantities of nanoparticles were added for the different types and sizes. For QDs, 3.00 fmol to 2.63 nmol were added per gram of tissue. For 17 nm gold nanoparticles, 2.92 to 2400.00 fmol were added per gram of tissue. For 28 nm gold nanoparticles, 0.81 to 675.00 fmol were added per gram of tissue. For 44 nm gold nanoparticles, 0.12 to 97.50 fmol were added per gram of tissue. For Fe_3O_4 nanoparticles, 0.0003 to 2.5750 nmol were added per gram of tissue. The amount of tissue added for QD samples was 0.20 g for heart and spleen samples, and 0.25 g for all other tissues. For all three sets of Au nanoparticle samples and Fe_3O_4 samples, 0.10 g of heart and spleen, 0.13 g of brain and lung, 0.20 g of kidney, and 0.25 g of liver, skin, and muscle were used. The mass of tissue used was proportional to the organ size present in the rat. The upper limits of nanoparticle addition, which are above the anticipated concentrations of organ accumulation, were dictated by the quantities of each nanoparticle available.

The experiments to determine the threshold of interference resulting from the tissues were conducted by maintaining a constant quantity of added nanoparticles in five data points of triplicate samples, and varying the quantity of liver homogenate added. Other organs were not used, as data from the first set of experiments with various tissues showed that the type of tissue used has no effect on detection sensitivity. The quantity of nanoparticles added differed between nanoparticle types, aiming for a detected value in the linear range demonstrated above, but close enough to the lower limit for interference to be observed. For QDs, 1.1 pmol was added to 0.25, 0.50, 1.00, 2.00, and 3.00 g of liver homogenate, and digested in 2.5 mL 70% HNO_3. For the gold nanoparticles, 8.1, 6.7, and 1.0 fmol of 17, 28, and 44 nm gold nanoparticles, respectively, were added to 0.075, 0.125, 0.250, 0.500, and 1.000 g liver homogenate. For Fe_3O_4, 0.78 pmol was added to 0.075, 0.125, 0.250, 0.500, and 1.000 g liver homogenate.

Sample Mineralization

For analysis, biological samples were dissolved completely in nitric acid, (70% *w/w*). All samples were prepared in disposable 25-ml glass culture tubes (Sigma) that were fitted with polyethylene "snap caps" (Fisher). For all ICP-AES measurements, nitric acid blanks, blank tissue samples, positive nanoparticle control calibration curves without tissue, and element standards were prepared and tested concurrently with test samples. After puncturing of the cap, the samples were digested in an oil bath at 110–120 °C for 2–3 h. Any remaining undissolved solids were removed by filtering through a 0.45-μm pore PVDF membrane syringe filter. The filtrate was rediluted to 5 ml with distilled water (DD-H_2O) and transferred to 15 ml polypropylene tubes.

ICP-AES Analysis

The analysis of all samples was conducted using a Perkin-Elmer Optima 3000 ICP-AES system. Digested samples were diluted to 5 ml, and one wavelength was used as an indicator for nanoparticle concentration (228.805, 267.595, and 238.204 nm for Cd I, Au I, and Fe II, respectively).

Aqueous calibration curves of Cd, Au, and Fe, prepared from certified elemental standards (High Purity Standards, Charleston SC, USA) and assayed at the same emission wavelength, were used for quantification under Instrumental analysis conditions outlined in Table 2.

Acknowledgments We thank Devika Chithrani for valuable assistance. This work was supported by CIHR, NSERC, CFI, OIT, and the University of Toronto. HF thanks NSERC, OGS, and the University of Toronto for fellowship support.

References

1. Gao X, Cui Y, Levenson RM, Chung LWK, Nie S. Nat Biotechnol 2004;22:969–76.
2. Hirsch LR, Stafford RJ, Bankson JA, Sershen SR, Rivera B, Price RE, et al. Proc Natl Acad Sci U S A 2003;100:13549–54.
3. Kim S, Lim YT, Soltesz EG, DeGrand AM, Lee J, Nakayama A, et al. Nat Biotechnol 2004;22:93–7.
4. Kostarelos K. Adv Colloid Interface Sci 2003;106:147–68.
5. Singh R, Pantarotto D, Lacerda L, Pastorin G, Klumpp C, Prato M, et al. Proc Natl Acad Sci U S A 2006;103:3357–62.
6. Shenoy D, Little S, Langer R, Amiji M. Pharm Res 2005;22:2107–14.
7. Hines MA, Guyot-Sionnest P. J Phys Chem B 1996;100:468–71.
8. Fischer HC, Liu L, Pang KS, Chan WCW. Adv Funct Mater 2006;16:1299–305.
9. Sun X, Rossin R, Turner JL, Becker ML, Joralemon MJ, Welch MJ, et al. Biomacromolecules 2005;6:2541–54.
10. Hoshino A, Fujioka K, Oku T, Suga M, Sasaki YF, Ohta T, et al. Nano Lett 2004;4:2163–9.
11. Ballou B, Lagerholm BC, Ernst LA, Bruchez MP, Waggoner AS. Bioconjug Chem 2004;15:79–86.
12. Jiang W, Papa E, Fischer H, Mardyani S, Chan WCW. Trends Biotechnol 2004;22:607–9.
13. Cheng F-Y, Su C-H, Yang Y-S, Yeh C-S, Tsai C-Y, Wu C-L, et al. Biomaterials 2005;26:729–38.
14. Jiang W, Mardyani S, Fischer H, Chan WCW. Chem Mater 2006;18:872–8.

15. Li Z, Chen H, Bao H, Gao M. Chem Mater 2004;16:1391.
16. Frens G. Nat Phys Sci 1973;241:20–2.
17. Freeman RG, Grabar KC, Allison KJ, Bright RM, Davis JA, Guthrie AP, et al. Science 1995;267:1629–32.
18. Yu WW, Qu L, Guo W, Peng X. Chem Mater 2003;15:2854–60.
19. Chithrani BD, Ghazani AA, Chan WCW. Nano Lett 2006;6:662–8.
20. Shackelford JF, Alexander W, editors. CRC Materials science and engineering handbook. 3rd ed. Boca Raton, FL: CRC; 2001.
21. Fearn D'ACB. Ann Rheum Dis 1973;32:34–7.
22. Saterborg NE. Acta Radiol Ther Phys Biol 1973;12:509–28.
23. Cook NJ, Wood SA, Zhang Y. J Geochem Explor 1992;46: 187–228.
24. Chao TT, Jenne EA, Heppting LM. US Geological Survey Prof Paper 1968;600D:D16–19.
25. Krachler M, Radner H, Irgolic KJ. Fresenius' J Anal Chem 1996;355:120–8.
26. Ciuffi M, Gentilini G, Franchi-Micheli S, Zilletti L. Neurochem Res 1992;17:1241–6.
27. Chen LH, Thacker RR. Int J Vitam Nutr Res 1986;56:253–8.
28. Cempel M. Biol Trace Elem Res 2004;102:198–198.
29. Herrera AP, Resto O, Briano JG, Rinaldi C. Nanotechnology 2005;16:S618–25.
30. Maye MM, Han L, Kariuki N, Ly NK, Chan W-B, Luo J, et al. Anal Chim Acta 2003;496:17–27.